

Thermal annealing behaviour and gel to crystal transition of a low molecular weight hydrogelator

Emily C. Barker,^a Adam D. Martin,^b Christopher J. Garvey,^c Ching Yong Goh,^a Franca Jones,^a Mauro Mocerino,^a Brian W. Skelton,^d Mark I. Ogden^{*a,e} and Thomas Becker^{*a,d}

Received 00th January 20xx,
Accepted 00th January 20xx

DOI: 10.1039/x0xx00000x

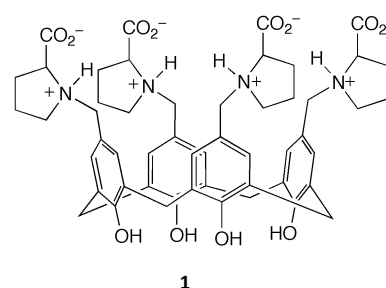
www.rsc.org/

The thermal annealing behaviour of an electrolyte-triggered calixarene hydrogelator is found to depend strongly on the specific metal chloride used. While the lithium chloride gel showed typical gel-sol transitions as a function of temperature, the magnesium chloride gel was found to repeatedly strengthen with heat-cool cycles. Structural investigations using small-angle neutron scattering, and scanning probe microscopy, suggest that the annealing behaviour is associated with a change in morphology of the fibrous structures supporting the gel. On prolonged standing at room temperature, the magnesium chloride gel underwent a gel-crystal transition, with the collapsing gel accompanied by the deposition of crystals of a magnesium complex of the proline-functionalised calix[4]arene gelator.

Introduction

Low molecular weight gelators (LMWGs) are attracting attention for their potential applications in areas including environmental remediation,¹ drug delivery,² personal care products,³ tissue engineering,^{2, 4} pharmaceutical crystallisation,⁵ catalysis,⁶ and numerous others.^{7, 8} LMWGs form supramolecular gels, where the sample spanning networks result from intermolecular non-covalent interactions that can include hydrogen-bonding, hydrophobic, π - π , and van der Waals interactions.^{9, 10} These networks can be readily influenced by external parameters, such as heat, light, pH, ionic strength and so on, inducing rapid and reversible changes in the gel.¹¹ Much of the effort in this area has focussed on moving the development of new LMWGs beyond serendipity,^{12, 13} with a few motifs and modifications now relatively well understood.¹⁴⁻¹⁸ Nevertheless, there remain many aspects of LMWG behaviour in need of investigation. For example, Adams¹⁹ has recently pointed out that the aging behaviour of supramolecular gels has not been widely explored, despite a significant number of examples showing that the gel state is not the thermodynamic minimum of the system. A number of recent reports emphasise that gel structures can indeed evolve over time, on standing,²⁰ or after treatment such as change in

temperature.^{21, 22} In some cases, a gel-crystal transition occurs and the gelator molecules crystallise directly from the gel,²³⁻²⁷ as distinct from cases where a gel is used as a matrix to control crystal growth.²⁸⁻³⁰ In these cases the gel is weakened or collapses completely as a result of the growth of the new crystalline phase. In other systems, gel aging involves Ostwald ripening where smaller fibres are lost in preference to larger and more stable structures over time, leading to a more robust gel.^{31, 32} Other gel systems may become more homogeneous over time after the initial formation of the network, again leading to a more robust gel.³³ A fascinating recent example of a gel-gel transition is a carbonate-triggered transition from an opaque to transparent dipeptide gel, accompanied by an increase in gel strength, explained by a transition from spherical to fibrous structures.¹⁹



We have previously reported that the proline-functionalised calix[4]arene, **1**, functions as a pH-sensitive electrolyte-triggered hydrogelator.³⁴ The structure of the fibrous network formed, as well as the stability of the gel, was found to vary with the electrolyte used. A gel-crystal transformation was also observed, albeit from a racemic mixture, which allowed the structural characterisation of a lanthanum-containing species.³⁵ This structure provided useful insight into how this molecule might stack to form high aspect ratio structures. We have also used this gelator system to develop methodology for using

^a Department of Chemistry and Nanochemistry Research Institute, Curtin University, GPO Box U1987, Perth, Western Australia 6845, Australia. Email: t.becker@curtin.edu.au, m.ogden@curtin.edu.au

^b School of Chemistry and the ARC Centre for Convergent Bio-Nano Science and Technology, The University of New South Wales, Sydney, NSW 2052, Australia.

^c Australian Nuclear Science and Technology Organisation, New Illawarra Rd, Lucas Heights, NSW, Australia, 2231.

^d Centre for Microscopy, Characterisation and Analysis, M310, The University of Western Australia, Crawley, Western Australia 6009, Australia.

^e School of Chemistry and Biochemistry, M310, The University of Western Australia, Crawley, Western Australia 6009, Australia

Electronic Supplementary Information (ESI) available: SANS data fitting, Atomic force micrographs of hydrogels. See DOI: 10.1039/x0xx00000x

scanning probe microscopy as an *in situ* technique for studying the assembly and disassembly of the fibrous structures as a function of temperature.³⁶ While carrying out these studies, we occasionally observed some structural changes occurring in the MgCl₂-1 gel system as the temperature was cycled. This prompted us to carry out a more detailed study of the response of this system to temperature cycling, including changes in the bulk rheology, as well as the gel structure. On standing for prolonged periods under ambient conditions, a gel-crystal transition was observed, and the nature of the crystalline material is also reported here.

Experimental

Calixarene **1** was prepared following the literature method.³⁴ All other materials were used as received.

Scanning Probe Microscopy

All atomic force microscopy (AFM) data were acquired with a Bruker Dimension FastScan AFM system. The raw AFM data were processed in terms of 1st order plane-fitting and 1st order flattening with the Bruker NanoScope Analysis software v1.50. The NanoScope Analysis software was further used to analyse cross sections and to export the images.

Freshly cleaved mica was used as substrate for all AFM experiments. *In-situ* AFM measurements were performed on a temperature controlled sample stage using PeakForce Tapping as reported previously.³⁶ The gel was imaged in a small droplet which was placed with a pipette on the freshly cleaved mica substrate. Bruker FastScan-B probes with a spring constant of 1 N/m were used for *in-situ* AFM imaging of the assembly and disassembly process of the gel.

Ex-situ AFM imaging was carried out on thin films of gels prepared by smearing the gel across a freshly cleaved mica substrate with a glass pipette. These films were imaged using standard Tapping Mode AFM with Bruker TESPAs probes with a spring constant of 42 N/m and a resonant frequency of 300 kHz.

Rheology

Rheological measurements were performed on an Anton Paar MCR 302 rheometer using a 25 mm stainless steel parallel plate geometry configuration and analysed using RheoPlus v3.61 software. Typical rheology measurements involved casting 550 μ L of either the MgCl₂-1 or LiCl-1 sol onto one of the stainless steel plates, lowering the other plate to the measurement position, and allowing two hours for the gel to form *via* cooling the system to 10 °C. A Peltier temperature control hood and solvent trap was used to reduce evaporation and maintain a temperature of 10 °C for frequency and amplitude sweeps. Frequency sweeps were performed with a log ramp frequency from 0.01 – 10 Hz and a constant strain of 0.2%. Amplitude Sweeps were performed with constant frequency of 1 Hz and a log ramp strain of 0.1 – 100%. Temperature ramps were undertaken at five degree intervals, with heating taking place over five minutes and the sample equilibrated for a further ten minutes. The rheology plots displayed are an average of at least

three repeats for each point and error bars denote two standard deviations from the log-averaged mean.

Small angle neutron scattering

Hydrogels were prepared with either MgCl₂ or LiCl and transferred to a demountable titanium cell of 2 mm path length before being left to set over four hours at 5 °C. Measurements were performed at detector distances of 2 and 14 m. Isotropic scattering patterns were radially averaged and combined for a q range of 0.005 – 0.35 \AA^{-1} , where $q = 4\pi\sin(\theta)/\lambda$, and λ is neutron wavelength (5 \AA with a wavelength spread, $\Delta\lambda/\lambda$ 12%) and 2θ is the scattering angle. Data was corrected for the background, empty cell scattering and the sensitivity of the individual detector pixels. The data was reduced using IgorPro software³⁷ employing NIST macros specific to QUOKKA³⁸ to an absolute intensity scale and modelled using SasView.³⁹

Crystallography

Crystals isolated from a MgCl₂-1 gel that underwent a gel-crystal transition after standing for a prolonged period under ambient conditions were found to be suitable for a single X-ray structure determination. Crystallographic data were collected on an Oxford Diffraction Gemini diffractometer using Cu K α radiation. Data were collected at 100(2) K. Following multi-scan absorption corrections and solution by direct methods, the structure was refined against F^2 with full-matrix least-squares using the program SHELXL-97.⁴⁰ Unless stated below, anisotropic displacement parameters were employed for all of the non-hydrogen atoms. Unless otherwise stated, hydrogen atoms were added at calculated positions and refined by use of riding models with isotropic displacement parameters based on those of the parent atoms. Crystallographic data for the structure reported in this paper have been deposited at the Cambridge Crystallographic Data Centre with supplementary publication numbers CCDC 1508883. Copies of the data can be obtained free of charge on application to CCDC, 12 Union Rd, Cambridge CB21EZ, UK (fax +441223336033; email deposit@ccdc.cam.ac.uk).

Crystal data and refinement details

Empirical formula C₅₂H₉₆Cl₂MgN₄O₃₀; formula weight 1352.54, tetragonal, space group $P4$; $a = 14.1242(1)$, $c = 16.6170(1)$ \AA , $V = 3314.98(4)$ \AA^3 , $Z = 2$, $D_c = 1.355$ Mg/m³, $\mu = 1.728$ mm⁻¹, crystal size 0.46 \times 0.25 \times 0.15 mm³; $\theta_{\text{min,max}}$, 2.66 to 67.13°, reflections collected 40081; independent reflections 5900 [$R_{\text{int}} = 0.0278$], data/restraints/parameters 5900/3/450, goodness-of-fit on F^2 1.091; final R indices [$I > 2\sigma(I)$] $R_1 = 0.0826$, $wR_2 = 0.2396$; R indices (all data) $R_1 = 0.0833$, $wR_2 = 0.2406$. One C atom of the proline ring for molecule 2 (C224) was found to be disordered over 2 sites (C224 and C227) with site occupancy factors refined to 0.64(2) and 1-0.64(2). The 2 largest non-bonded peaks in the difference maps were modelled as Cl⁻ ions, both being situated on crystallographic 2-fold axes. The remaining peaks were modelled as O atoms of water molecules with site occupancies set at either 0.5 or 1.0 after trial refinement. Solvent and coordinated water molecule H atoms were not located.

Results and discussion

Oscillatory rheology measurements on $\text{MgCl}_2\cdot\mathbf{1}$ and $\text{LiCl}\cdot\mathbf{1}$ show that these gels display different stiffnesses, with storage moduli (G') of 5×10^4 Pa and 8×10^2 Pa respectively, Fig. 1a. This suggests that the selection of electrolyte plays a key role in tuning the strength of the resultant hydrogel, as reported previously.^{34, 35} Strain sweeps of these gels reveal that their strain dependent behaviour is also dependent on the choice of electrolyte, Fig. 1b. Hydrogels of $\text{MgCl}_2\cdot\mathbf{1}$ are relatively brittle, with deformation from the linear viscoelastic region occurring above strains of 0.3%, whereas this is extended for $\text{LiCl}\cdot\mathbf{1}$ gels to 2%.

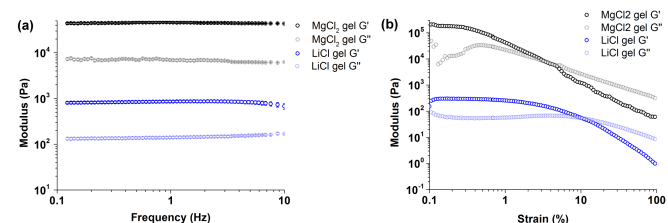


Fig. 1 – Oscillatory rheology frequency sweep (a) and strain sweep (b) measurements of $\text{MgCl}_2\cdot\mathbf{1}$ and $\text{LiCl}\cdot\mathbf{1}$ hydrogels. Gels were prepared using a 20 mM concentration of **1** and measured at 10 °C.

Next, the temperature dependent rheological behaviour of these hydrogels was investigated. It was macroscopically observed that hydrogels of **1**, regardless of the metal salt used, underwent a reversible gel-sol transition at approximately 25 °C. For $\text{LiCl}\cdot\mathbf{1}$ hydrogels, it can be seen that upon heating from 10 to 30 °C, these hydrogels drastically weaken above 20 °C, consistent with the observed gel-sol transition. This transition is reversible upon cooling, however, with this sol-gel transition observed over multiple cycles (Fig. 2a). The $\text{MgCl}_2\cdot\mathbf{1}$ hydrogels however, exhibit significantly different behaviour. Upon heating to 30 °C, these gels increase in strength, before maintaining this increased stiffness upon cooling (Fig. 2b). This type of annealing behaviour is rarely reported for supramolecular hydrogels,^{21, 22} but is more commonly observed in polymeric gels.⁴¹⁻⁴⁶ It should be noted that this increase in hydrogel strength is a reproducible phenomenon and there is no apparent loss of water upon heating. Over three heating cycles, the gel strength increases over an order of magnitude, however the increases in gel stiffness get smaller over repeated annealing cycles (see Figure S1). These results suggest that a dynamic rearrangement process is occurring for $\text{MgCl}_2\cdot\mathbf{1}$ hydrogels as the temperature is increased, with this new structure likely being “frozen in” upon the decrease in temperature.

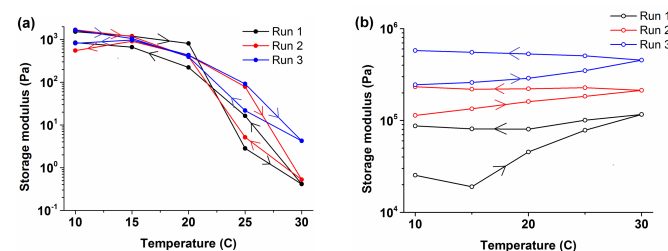


Fig. 2 – Temperature dependent behaviour $\text{LiCl}\cdot\mathbf{1}$ gels (a) and $\text{MgCl}_2\cdot\mathbf{1}$ gels (b). The temperature was cycled three times between 10 and 30 °C in five degree intervals, with a calixarene concentration of 20 mM used.

Atomic force microscopy was used to further investigate this annealing behaviour. We initially carried out *in situ* AFM measurements of the $\text{MgCl}_2\cdot\mathbf{1}$ gel, following our previously reported method.³⁶ This showed that fibres of a different morphology began forming after heating the sample to 25-30 °C (see Figure 4). The new fibres are larger in diameter (~ 20 nm) and straighter than the fibres formed originally, which are ~ 1 nm in diameter. On heating, the smaller diameter fibres apparently dissolve more readily than the thicker fibres (Figure 4(c)), suggesting a possible mechanism for the annealing behaviour, assuming that these thicker fibres are supporting the formation of a more robust gel. Unfortunately, more extensive temperature cycling was difficult to achieve as the gel became opaque preventing imaging.

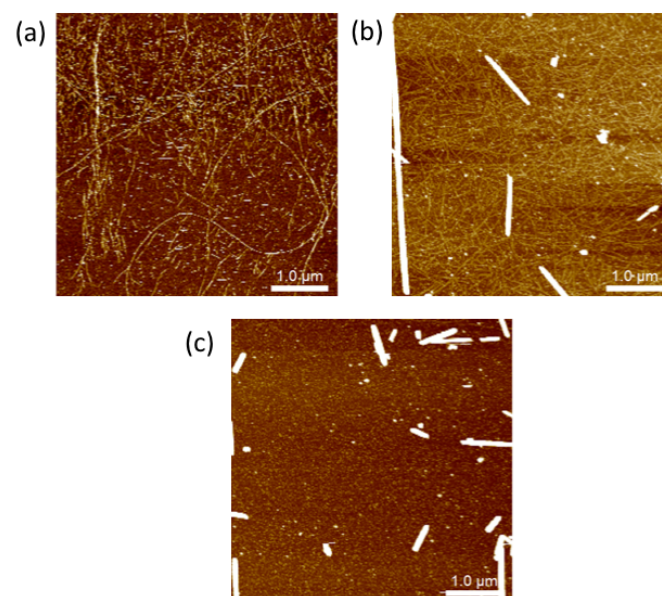


Figure 4. Scanning probe micrographs of a $\text{MgCl}_2\cdot\mathbf{1}$ gel imaged *in situ* on a mica substrate. (a) The gel after initial formation at room temperature (z-scale, 5 nm). (b) The gel after being heated to 25 °C (z-scale, 15 nm). (c) The gel after heating to 30 °C (z-scale, 15 nm).

To examine the $\text{MgCl}_2\cdot\mathbf{1}$ gel over more temperature cycles, *ex situ* AFM measurements were carried out. Bulk samples were heat cycled and then a sample of gel smeared on to a mica substrate for imaging after each cycle. The temperature range used in this case was room temperature (~ 22 °C) to 50 °C, as the lower temperatures produced samples that were difficult to apply to the substrate reproducibly. The resulting sequence of images for the $\text{MgCl}_2\cdot\mathbf{1}$ gel is shown in Figure S2. These images show similar changes, with the long thin fibres initially observed being replaced by straighter fibres after being heated and cooled. The gel fibres are somewhat shorter and straighter than observed in the initially formed gel consistent with the *in situ* measurements.

In comparison, the $\text{LiCl}\cdot\mathbf{1}$ gel was able to be imaged more successfully *in situ*, with the gel remaining transparent and the

fibres deposited apparently unchanged after each heat cycle, with similar fibre lengths and curvature (Figure S3). In this system, the challenge with *in situ* imaging was the tendency of the gel fibres to form rapidly once the process commenced. Within these constraints, the results obtained were consistent with the rheology results, in that the fibre formation was reversible. Similarly, *ex situ* experiments with the LiCl·1 gel did not show any clear change in the fibre structures with heat cycling (Figure S4).

This annealing behaviour was then examined using small angle neutron scattering (SANS). Hydrogel samples of both MgCl₂·1 and LiCl·1 were studied over a temperature range of 10 – 30 °C. For LiCl·1, significant changes in the scattering pattern start to occur as soon as heating takes place, (Fig. 3a). For both LiCl·1 and MgCl₂·1, the scattering data was fitted to a flexible cylinder model (see Figures S5 and S6 for model fits to data), which is a physically realistic model based upon AFM data (see above), or a flexible cylinder and power law model for data obtained at higher temperatures. The power law model indicates a change from uniform rod-like structures to a more complex system, which is also observed through AFM measurements. The outputs for two annealing cycles can be seen in Table 1, which shows that upon crossing T_g , the gel transition temperature, there is a significant drop in the length of the fibres. Importantly, for LiCl·1, the Kuhn length, which can be thought of as the length of a straight section of the fibre, is initially much lower than the fibre length, then becomes comparable to fibre length upon heating, before finally returning to being much lower than the fibre length. Physically, this represents an initial configuration of long, flexible fibres which become short, straight fibres upon heating, before transforming back to long, flexible fibres when the system is cooled. This is supported by *ex situ* AM images (Fig. S4)

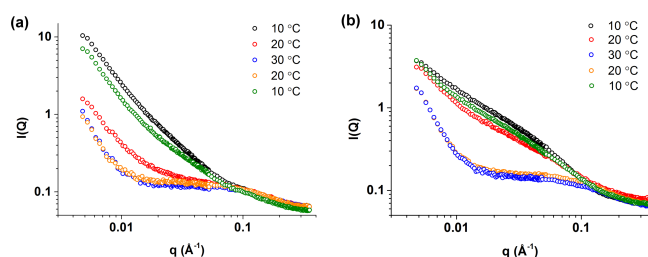


Fig. 3 – Scattering profiles obtained from SANS measurements for gels of LiCl·1 (a) and MgCl₂·1 (b) upon cycling the temperature from 10 – 30 – 10 °C. For these measurements, a calixarene concentration of 20 mM was used. Data is plotted on an absolute intensity scale (cm⁻¹).

The SANS results from hydrogels of MgCl₂·1 (Fig. 3b) upon annealing display a trend similar to that observed for LiCl·1, where the initial state for these gels is long, flexible fibres (large fibre size and small Kuhn length). Upon heating, the fibre size is shortened, similar to that observed for the LiCl·1 hydrogels. It should be noted here that the length of the fibres may also be the length between cross-links, rather than the absolute length of the fibre. Upon cooling however, as the fibre length increases the Kuhn length also increases, which is not observed for LiCl·1 gels. This indicates the formation of long,

straight fibres, compared to the long flexible fibres seen for LiCl·1. This straightening upon annealing is supported by *ex situ* AFM images (Fig. S2). The fibre radius obtained when modelling the SANS data (Table S1) does not significantly change over the course of the annealing experiments. This is contrary to AFM measurements, which show the presence of larger (20 nm) fibres upon heating (Fig. 4), which persist upon repeated annealing cycles (Fig. S2 and S4). These large fibres are unable to be observed by SANS over the q range studied, but despite this, the data clearly suggest that the response of the two systems to heat cycling is different, with the MgCl₂·1 system exhibiting significant hysteresis.

Table 1 – Outputs obtained from fitting SANS data on hydrogels to flexible cylinder model. All sizes given are in Angstroms.

T (°C)	LiCl·1 gel		MgCl ₂ ·1 gel	
	Kuhn length	Length	Kuhn length	Length
10	47 ± 1	Inf	40 ± 1	399 ± 1
15	80 ± 2	965 ± 35	60 ± 2	308 ± 5
20	60 ± 1	53 ± 1	260 ± 134	271 ± 58
25	37 ± 11	32 ± 1	175 ± 2	159 ± 2
30	38 ± 6	33 ± 1	48 ± 4	42 ± 3
25	49 ± 3	35 ± 1	44 ± 11	38 ± 1
20	39 ± 10	34 ± 1	42 ± 8	36 ± 1
15	48 ± 9	37 ± 1	237 ± 12	217 ± 20
10	78 ± 2	781 ± 18	228 ± 20	288 ± 20

While Ostwald ripening behaviour of gel systems has been reported previously over periods of days,^{31, 32} here we did not observe strengthening of the gels on standing at room temperature. In fact, regardless of whether the gels were heat-cycled, or left to stand at room temperature, both the LiCl·1 and MgCl₂·1 gels collapsed on standing for 10-20 days, depositing crystalline or microcrystalline materials. In the case of the MgCl₂·1 gel, in some cases crystals were found to be of sufficient quality for a single crystal structure determination. The results were consistent with the formulation [Mg(1)(OH₂)₂]Cl₂·16H₂O. There are 2 crystallographically independent, but similar, cations in the unit cell with the Mg atoms on crystallographic 4-fold axes in space group *P4*. Thus, only one quarter of each molecule is independent. The coordination around the Mg atom is octahedral, with two *trans* water O atoms, and four carboxylate acid O atoms in the remaining positions (Figure 5). The phenolic O atoms display the typical cyclic hydrogen bond array. The proline moieties are zwitterionic, with hydrogen bonds between the protonated N atoms, and the neighboring carboxylate O atoms (Figure 5), to form a second intramolecular cyclic array. This structure is quite different to the lanthanum salt of the racemate reported previously. In that structure, the calixarene cavity was occupied by a neighboring proline moiety generating an inclusion polymer along a 2-fold screw axis.³⁵ This structure presented a possible motif by which this gelator could generate high aspect ratio structures. Here, the calixarene cavity is occupied by the coordinated Mg(OH₂)₂²⁺ entity, with no obvious directional intermolecular interactions. This is a reminder that crystal

packing need not have any resemblance to intermolecular interactions in a gel, and underlines the need to develop high resolution imaging of gel networks to provide direct evidence of packing interactions.

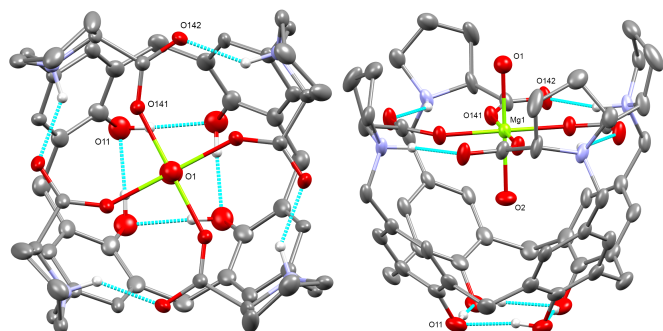


Figure 5. Two views of molecule 1 in the crystal structure $[Mg(1)(OH_2)_2]Cl_2 \cdot 16H_2O$. (a) The view orthogonal to the phenol O4 plane, and (b) a view tilted to highlight the inclusion of the Mg cation and associated aqua ligands in the calixarene cavity. Hydrogen atoms not involved in the hydrogen bonds, and atoms of the minor components of the disorder have been omitted. Displacement ellipsoids are at the 30% probability level.

Conclusions

The hydrogel formed by combining proline-functionalised calixarene **1** with magnesium chloride was found to increase in strength as temperature was cycled. This annealing behaviour was not observed when magnesium chloride was replaced with lithium chloride. SANS and AFM measurements demonstrated that the change in rheological properties is induced by a change in the gel fibre morphology to thicker straighter fibre assemblies. Similar changes in fibre structure did not occur with the lithium chloride gel, consistent with the rheological results. Prolonged standing at room temperature did not induce similar changes in the $MgCl_2$ -**1** gel. Instead the gels tended to undergo a gel to crystal transition. This crystalline phase had no structural features to suggest that the intermolecular interactions in the crystal were similar to those giving rise to the gel fibres. The driving force behind the changes observed in the $MgCl_2$ -**1** gel as a result of temperature changes requires further investigation.

Acknowledgements

We acknowledge use of the facilities and scientific and technical assistance of the Australian Microscopy and Microanalysis Research Facility at the Centre for Microscopy, Characterisation, and Analysis, The University of Western Australia, and at the Centre for Microscopy and Microanalysis, University of Queensland, a facility funded by the University, State and Commonwealth Governments. We also acknowledge Mr Brendan Ennis for assistance with synthesis of the proline functionalised calixarene. We thank the Australian Nuclear Science and Technology Organisation (ANSTO) for access to the QUOKKA SANS beamline (proposal 4934). ADM acknowledges the National Health and Medical Research Council for the award

of a Dementia Research Development Fellowship (APP1106751).

Notes and references

1. B. O. Okesola and D. K. Smith, *Chem. Soc. Rev.*, 2016, **45**, 4226-4251.
2. K. J. Skilling, F. Citossi, T. D. Bradshaw, M. Ashford, B. Kellam and M. Marlow, *Soft Matter*, 2014, **10**, 237-256.
3. B. O. Okesola, V. M. P. Vieira, D. J. Cornwell, N. K. Whitelaw and D. K. Smith, *Soft Matter*, 2015, **11**, 4768-4787.
4. X. W. Du, J. Zhou, J. F. Shi and B. Xu, *Chem. Rev.*, 2015, **115**, 13165-13307.
5. J. A. Foster, M. O. M. Piepenbrock, G. O. Lloyd, N. Clarke, J. A. K. Howard and J. W. Steed, *Nat. Chem.*, 2010, **2**, 1037-1043.
6. D. D. Diaz, D. Kuhbeck and R. J. Koopmans, *Chem. Soc. Rev.*, 2011, **40**, 427-448.
7. M. O. M. Piepenbrock, G. O. Lloyd, N. Clarke and J. W. Steed, *Chem. Rev.*, 2010, **110**, 1960-2004.
8. A. R. Hirst, B. Escuder, J. F. Miravet and D. K. Smith, *Angew. Chem. Int. Ed.*, 2008, **47**, 8002-8018.
9. L. A. Estroff and A. D. Hamilton, *Chem. Rev.*, 2004, **104**, 1201-1217.
10. R. G. Weiss, *J. Am. Chem. Soc.*, 2014, **136**, 7519-7530.
11. S. J. Wezenberg, C. M. Croisetu, M. C. A. Stuart and B. L. Feringa, *Chem. Sci.*, 2016, **7**, 4341-4346.
12. D. M. Zurcher and A. J. McNeil, *J. Org. Chem.*, 2015, **80**, 2473-2478.
13. J. K. Gupta, D. J. Adams and N. G. Berry, *Chem. Sci.*, 2016, **7**, 4713-4719.
14. C. Tomasini and N. Castellucci, *Chem. Soc. Rev.*, 2013, **42**, 156-172.
15. K. K. Diehn, H. Oh, R. Hashemipour, R. G. Weiss and S. R. Raghavan, *Soft Matter*, 2014, **10**, 2632-2640.
16. J. A. Foster, R. M. Edkins, G. J. Cameron, N. Colgin, K. Fucke, S. Ridgeway, A. G. Crawford, T. B. Marder, A. Beeby, S. L. Cobb and J. W. Steed, *Chem. Eur. J.*, 2014, **20**, 279-291.
17. M. Ikeda, T. Tanida, T. Yoshii and I. Hamachi, *Adv. Mater.*, 2011, **23**, 2819-2822.
18. Y. Q. Lan, M. G. Corradini, X. Liu, T. E. May, F. Borondics, R. G. Weiss and M. A. Rogers, *Langmuir*, 2014, **30**, 14128-14142.
19. E. R. Draper, T. O. McDonald and D. J. Adams, *Chem. Commun.*, 2015, **51**, 6595-6597.
20. A. Baral, S. Basak, K. Basu, A. Dehsorkhi, I. W. Hamley and A. Banerjee, *Soft Matter*, 2015, **11**, 4944-4951.
21. H. Kumari, S. E. Armitage, S. R. Kline, K. K. Damodaran, S. R. Kennedy, J. L. Atwood and J. W. Steed, *Soft Matter*, 2015, **11**, 8471-8478.
22. S. Farrell, D. DiGuiseppi, N. J. Alvarez and R. Schweitzer-Stenner, *Soft Matter*, 2016, **12**, 6096-6110.
23. J. R. Moffat and D. K. Smith, *Chem. Commun.*, 2008, 2248-2250.
24. D. J. Adams, K. Morris, L. Chen, L. C. Serpell, J. Bacsá and G. M. Day, *Soft Matter*, 2010, **6**, 4144-4156.
25. Y. J. Wang, L. M. Tang and J. Yu, *Cryst. Growth Des.*, 2008, **8**, 884-889.

26. Y. Xu, C. Q. Kang, Y. Chen, Z. Bian, X. P. Qiu, L. X. Gao and Q. X. Meng, *Chem. Eur. J.*, 2012, **18**, 16955-16961.
27. W. Liyanage, W. W. Brennessel and B. L. Nilsson, *Langmuir*, 2015, **31**, 9933-9942.
28. E. Asenath-Smith, H. Y. Li, E. C. Keene, Z. W. Seh and L. A. Estroff, *Adv. Funct. Mater.*, 2012, **22**, 2891-2914.
29. D. K. Kumar and J. W. Steed, *Chem. Soc. Rev.*, 2014, **43**, 2080-2088.
30. S. Gao, S. Wang, J. Ma, Y. Wu, X. Fu, R. K. Marella, K. Liu and Y. Fang, *Langmuir*, 2016, DOI: 10.1021/acs.langmuir.6b03375.
31. M. Lescanne, P. Grondin, A. d'Aleo, F. Fages, J. L. Pozzo, O. M. Monval, P. Reinheimer and A. Colin, *Langmuir*, 2004, **20**, 3032-3041.
32. S. A. Jamieson, K. W. K. Tong, W. A. Hamilton, L. L. He, M. James and P. Thordarson, *Langmuir*, 2014, **30**, 13987-13993.
33. M. M. Smith and D. K. Smith, *Soft Matter*, 2011, **7**, 4856-4860.
34. T. Becker, C. Y. Goh, F. Jones, M. J. McIldowie, M. Mocerino and M. I. Ogden, *Chem. Commun.*, 2008, 3900-3902.
35. C. Y. Goh, T. Becker, D. H. Brown, B. W. Skelton, F. Jones, M. Mocerino and M. I. Ogden, *Chem. Commun.*, 2011, **47**, 6057-6059.
36. E. C. Barker, C. Y. Goh, F. Jones, M. Mocerino, B. W. Skelton, T. Becker and M. I. Ogden, *Chem. Sci.*, 2015, **6**, 6133-6138.
37. S. R. Kline, *J. Appl. Crystallogr.*, 2006, **39**, 895-900.
38. J. S. Pedersen and P. Schurtenberger, *Macromolecules*, 1996, **29**, 7602-7612.
39. SasView for Small Angle Scattering Analysis, <http://www.sasview.org/>.
40. G. M. Sheldrick, *Acta Crystallogr A*, 2015, **71**, 3-8.
41. A. V. Zhukhovitskiy, M. Z. Zhong, E. G. Keeler, V. K. Michaelis, J. E. P. Sun, M. J. A. Hore, D. J. Pochan, R. G. Griffin, A. P. Willard and J. A. Johnson, *Nat. Chem.*, 2016, **8**, 33-41.
42. R. C. Huber, A. S. Ferreira, J. C. Aguirre, D. Kilbride, D. B. Toso, K. Mayoral, Z. H. Zhou, N. Kopidakis, Y. Rubin, B. J. Schwartz, T. G. Mason and S. H. Tolbert, *J. Phys. Chem. B*, 2016, **120**, 6215-6224.
43. D. R. Griffin, W. M. Weaver, P. O. Scumpia, D. Di Carlo and T. Segura, *Nat. Mater.*, 2015, **14**, 737-744.
44. B. C. Wu and D. J. McClements, *J. Phys. D: Appl. Phys.*, 2015, **48**, 434002.
45. C. M. R. Perez, L. A. Rank and J. Chmielewski, *Chem. Commun.*, 2014, **50**, 8174-8176.
46. S. M. Bai, W. M. Zhang, Q. Lu, Q. H. Ma, D. L. Kaplanad and H. S. Zhu, *J. Mater. Chem. B*, 2014, **2**, 6590-6600.